

ROM SAF Report 47
Ref: SAF/ROM/METO/REP/RSR/047
Web: <https://rom-saf.eumetsat.int/>
Date: 19 June 2025



ROM SAF Report 47

An initial assessment of the quality of RO data from FY-3E

Owen Lewis

Met Office, Exeter, UK

DOCUMENT AUTHOR TABLE

	Author(s)	Function	Date
Prepared by:	Owen Lewis	ROM SAF Scientist	22/10 2024
Reviewed by (internal):	Neill Bowler	ROM SAF Local Manager	10/6 2025
Reviewed by (internal):	Sean Healy	ROM SAF Science Coordinator	9/5 2025
Approved by:	Kent Bækgaard Lauritsen	ROM SAF Project Manager	19/6 2025

DOCUMENT CHANGE RECORD

Version	Date	By	Description
1.0	19/06/2025	OL	Final version following internal reviews

ROM SAF

The Radio Occultation Meteorology Satellite Application Facility (ROM SAF) is a decentralised processing centre under EUMETSAT which is responsible for operational processing of radio occultation (RO) data from the Metop, Metop-SG and Sentinel-6 satellites and radio occultation data from other missions. The ROM SAF delivers bending angle, refractivity, temperature, pressure, humidity, and other geophysical variables in near real-time for NWP users, as well as reprocessed Climate Data Records (CDRs) and Interim Climate Data Records (ICDRs) for users requiring a higher degree of homogeneity of the RO data sets. The CDRs and ICDRs are further processed into globally gridded monthly-mean data for use in climate monitoring and climate science applications.

The ROM SAF also maintains the Radio Occultation Processing Package (ROPP) which contains software modules that aid users wishing to process, quality-control and assimilate radio occultation data from any radio occultation mission into NWP and other models.

The ROM SAF Leading Entity is the Danish Meteorological Institute (DMI), with Cooperating Entities: i) European Centre for Medium-Range Weather Forecasts (ECMWF) in Reading, United Kingdom, ii) Institut D'Estudis Espacials de Catalunya (IEEC) in Barcelona, Spain, iii) Met Office in Exeter, United Kingdom, and iv) and Wegener Center, University of Graz, in Graz, Austria. To get access to our products or to read more about the ROM SAF please go to: <https://rom-saf.eumetsat.int>

Intellectual Property Rights

All intellectual property rights of the ROM SAF products belong to EUMETSAT. The use of these products is granted to every interested user, free of charge. If you wish to use these products, EUMETSAT's copyright credit must be shown by displaying the words "copyright (year) EUMETSAT" on each of the products used.

Abstract

Feng-Yun 3E is a satellite flown by The Chinese Meteorological Agency (CMA) and the National Remote Sensing Centre of China (NRSCC). The satellite was launched on the 4th July 2021 in a sun synchronous orbit. On board the satellite has a GNSS Radio Occultation Sounder – 2 (GNOS2) instrument measuring the phase delay between a GNSS satellite and the low earth orbiting satellite. Observations from the GNOS2 instrument were first received over the Global Telecommunications system in March 2024.

The performance of the bending angles and the refractivity from FY-3E have been assessed and compared to similar observations such as those from FY-3D and Metop-C. Overall the quality of observations is similar to that seen from other operational instruments. The bending angle observations indicated an improved standard deviation above 35 km compared to FY-3D but there was a greater positive bias above 50 km for rising occultations. For refractivity bias increases above 30 km as is seen for FY-3D and Metop-C. This bias is smaller than that seen in FY-3D.

An experiment assimilating FY-3E into the Met Office's Global model system was also conducted. The results of this experiment indicate that the inclusion of FY-3E Bending Angle observations had a neutral to slightly negative impact.

Timeliness of FY-3E observations being disseminated on the GTS during September were slower when compared with FY-3D and Metop-C. Around half of the received observations from FY-3E would miss the global model assimilation cut-off.

List of Contents

1.	Bending angle evaluation	6
1.1	BIAS AND STANDARD DEVIATION CHARACTERISTICS	6
1.2	VERTICAL CORRELATIONS	9
2.	Refractivity assessment.....	11
3.	Assimilation test	14
4.	Other notable features.....	16
5.	Conclusion	17
6.	References.....	18

1. Bending angle evaluation

Global Navigation Satellite System Radio Occultation observations from Feng-Yun 3E (FY-3E) have been received via the GTS since 5th March 2024. Data arrival has been stable since this date. The satellite is flown by The Chinese Meteorological Agency (CMA) and the National Remote Sensing Centre of China (NRSCC).

FY-3E has a GNSS Radio Occultation sounder 2 (GNOS2) on board. This instrument measures the phase delay between the GNSS satellite and the low earth orbiting satellite, the instrument is located where the antenna is pointing both fore and aft. The instrument also contains another antenna which is pointing down to measure reflections from the sea surface and when co-processed alongside the precision-orbit-determination antennae a wind speed can be inferred. The GNOS2 instrument can receive signals from the GPS, Galileo, Glonass and BeiDou constellations, although only observations from GPS and BeiDou are currently being provided.

1.1 Bias and standard deviation characteristics

The normalised difference between the bending angle observations and the background model forecast from the Met Office's operational global numerical weather prediction (NWP) model are shown in Figure 1.1.

To calculate the mean and standard deviation the following formulae are used

$$\mu = \frac{1}{N} \sum_{i=1}^N \frac{O_i - B_i}{B_i} \quad (1.1)$$

$$\sigma = \sqrt{\frac{1}{N} \sum_{i=1}^N \left(\frac{O_i - B_i}{B_i} - \mu \right)^2} \quad (1.2)$$

where O_i and B_i are the observed and model background values for occultation i in the period with an overall total of N occultations. Statistics from FY-3E are compared with FY-3D and Metop-C in Figure 1.1. The bias between FY-3E and Metop-C are near identical with the exceptions of below 5 km and above approximately 54 km. Below 5 km FY-3E has a marginally smaller negative bias than Metop-C. Above 54 km FY-3E has a slightly larger positive bias compared with Metop-C. When comparing FY-3E to FY-3D again they are near identical until around 54 km where their biases diverge with FY-3E having a positive bias and FY-3D moving to have a negative bias. The negative bias in FY-3D reflects a known issue with setting occultations due to the antenna placement on this satellite.

Standard deviations between FY-3E and FY-3D are very similar with FY-3E having a slightly higher standard deviation above 35 km. When looking at the standard deviation between FY-3E and Metop-C there is noticeable increase in standard deviation for FY-3E

between 20-25 km which is also present in FY-3D. The height of 25 km is where CMA switches from processing the observations using geometric optics to using wave optics. The jump in the standard deviation indicates that the smoothing parameters for geometric and wave optics are not well matched at this boundary. Above 35 km the standard deviation for FY-3E is larger than that of Metop-C.

During this three month time period FY-3E provided a substantially larger number of observations than FY-3D, the difference being around 18000 observations. The number of observations from FY-3E is greater than Metop-C with an extra 5000 observations during this 3 month period. These extra observations can be attributed to receiving occultations from both GPS and BeiDou. The number of occultations for FY-3E received from GPS and BeiDou can be seen in Figure 1.2, with GPS providing 546 more occultations during this monitoring period. There is a noticeable decrease in the number of used bending angles from BeiDou above 30 km.

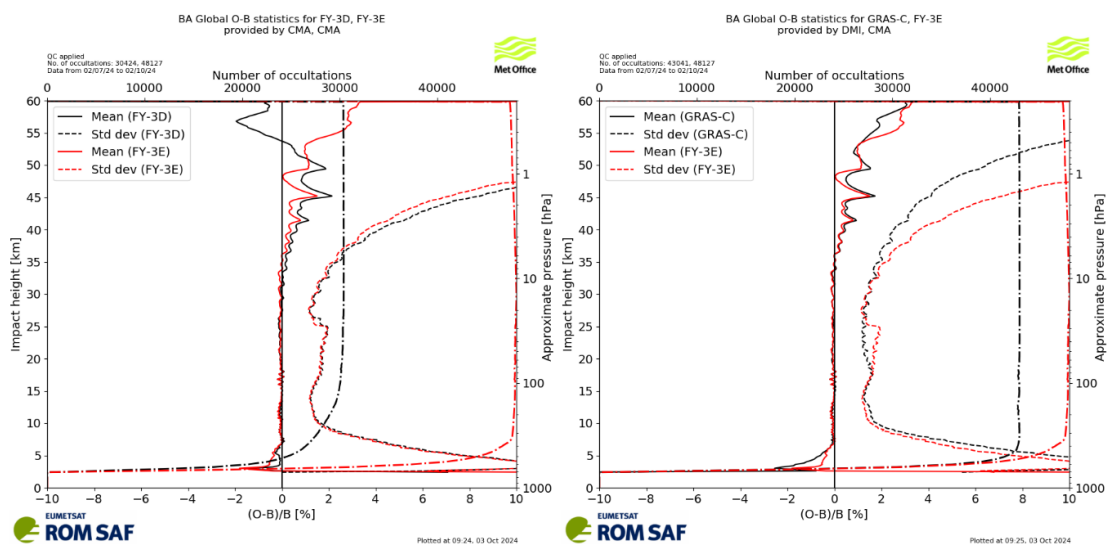


Figure 1.1: The bias and standard deviation of the normalised difference between the observation and the NWP model background forecast $(O-B)/B$ for bending angle from 02/07/2024 to 02/10/2024. Left is FY-3D vs FY-3E and right is Metop-C vs FY-3E.

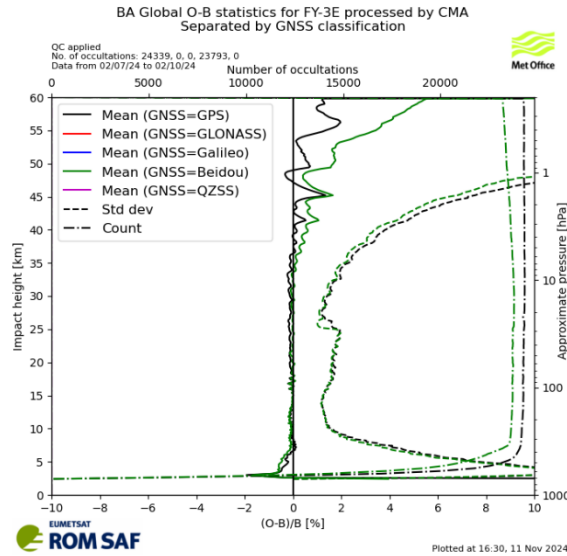


Figure 1.2: The bias, standard deviation and occultation counts of the normalised difference between the observation and the NWP model background forecast $(O-B)/B$ broken down by GNSS classification for bending angle from FY-3E. Calculated over the time period 02/07/2024 to 02/10/2024.

The rising and setting statistics for FY-3E compared to FY-3D and Metop-C are shown in Figure 1.3. Comparing to Metop-C, the bias of FY-3E rising occultations above 50 km are noticeably larger than the other observations. Above 55 km the FY-3E occultations have a smaller positive bias than Metop-C's setting occultations. As seen in the overall statistics in Figure 1.1 the standard deviation of FY-3E is larger between 20 and 25 km compared to Metop-C and also larger above 35 km. FY-3E has a smaller standard deviation above 35 km than FY-3D. FY-3E has the largest number of setting observations with over half of FY-3E observations coming from setting occultations. There is a noticeable decrease in the number of setting observations for FY-3E available with altitude above 30 km. The higher altitude decrease in occultations appears to come from a reduction in the number of BeiDou observations above 30 km as seen in Figure 1.2. This decrease in the number of observations above 30 km also corresponds with an increase in the standard deviations of the setting observations above 30 km compared to the FY-3E rising occultations.

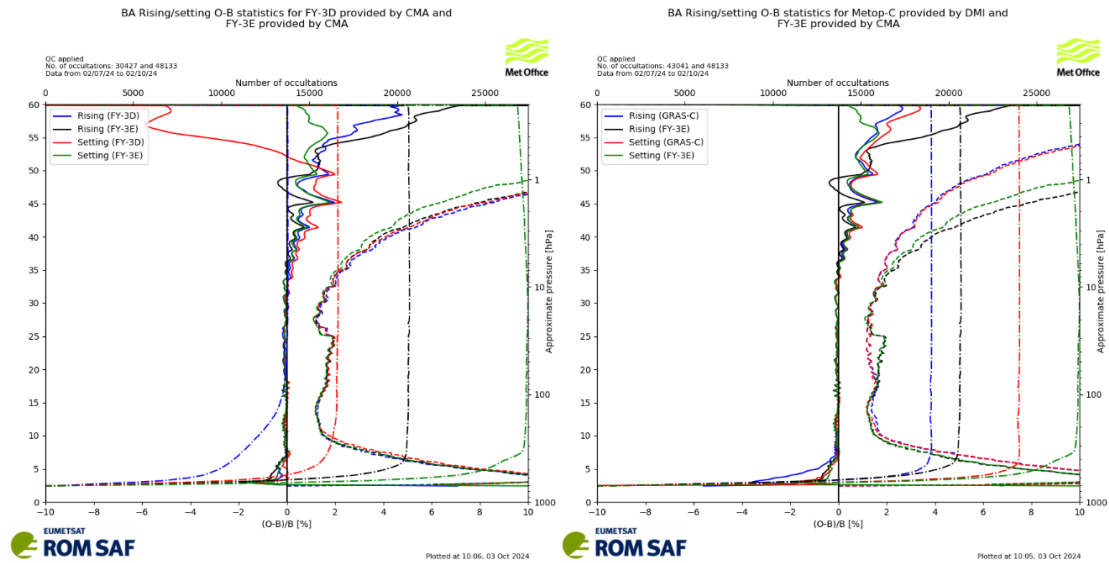


Figure 1.3: The bias and standard deviation of the normalised difference between the observation and the NWP model background forecast $(O-B)/B$ for bending angle broken down into the rising and setting occultations. Left is FY-3D vs FY-3E and right is Metop-C vs FY-3E.

1.2 Vertical correlations

At the Met Office when bending angles are assimilated into the NWP system an assumption is made that the error in each of the bending angle measurements is independent of the errors in every other measurement. Following on from this assumption we would therefore like the vertical observation-error covariance matrix \mathbf{R} to be diagonal, and the vertical correlations of $O-B$ to be close to diagonal, which can only be the case if there is no vertical correlation in the \mathbf{B} matrix. The vertical error correlations of the normalised innovations $(O-B)/B$ are shown in Figure 1.3 for both FY-3E, FY-3D and Metop-C. As bending angles are calculated as a smoothed difference between Doppler shifts, we can expect a region of positive correlations near the diagonal and negative correlations at further distances from the diagonal.

Vertical correlation patterns for FY-3D and FY-3E are very similar. There is a transition in behaviour around 26 km which is seen in both, which was noted previously for FY-3D in Bowler (2019) as being likely due to the transition from using geometric optics to wave optics. There are long range vertical correlations between heights of 10-26 km, and these are larger for FY-3D. Above 26 km the pattern for FY-3E is very similar to that which is seen for Metop-C.

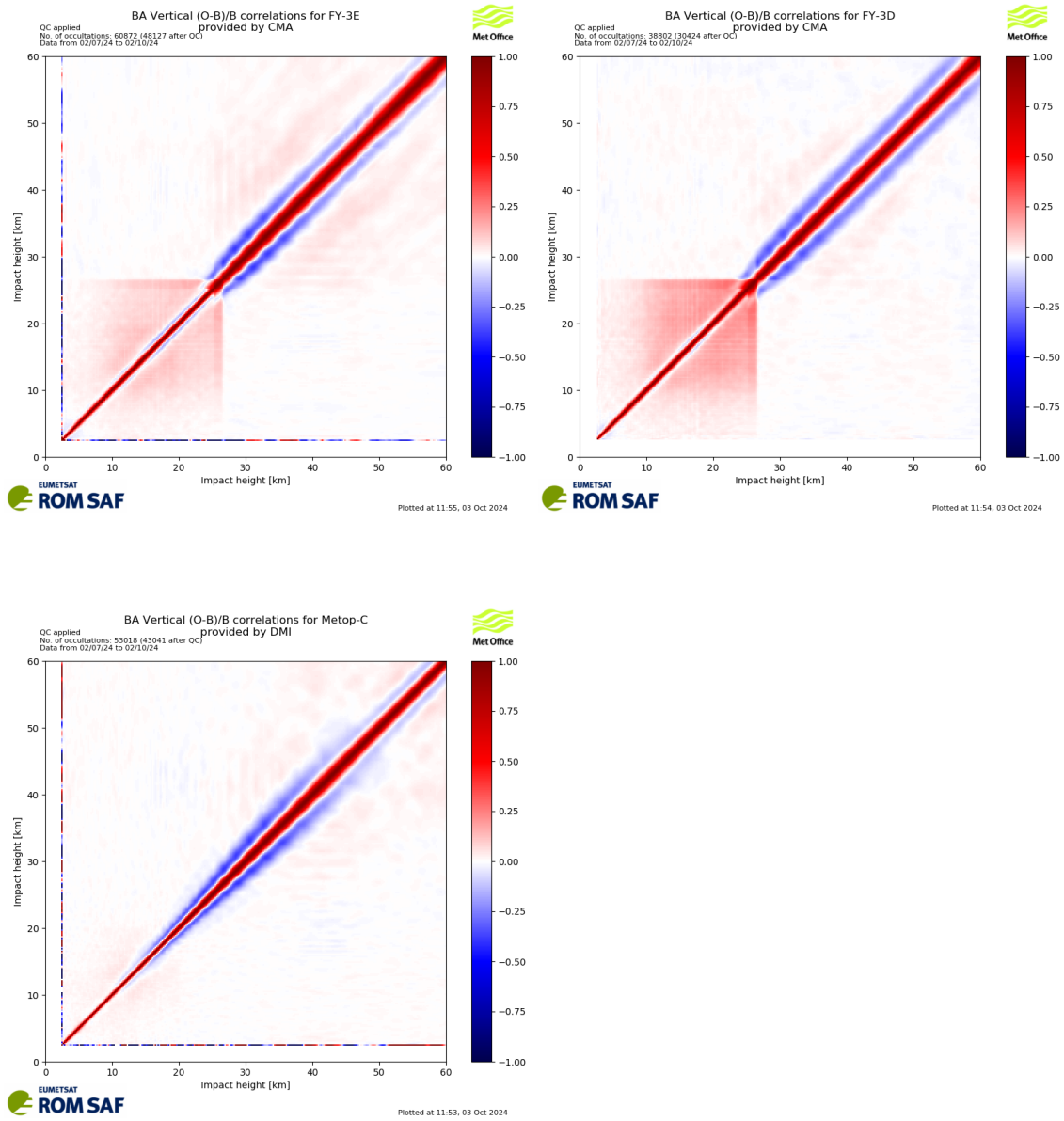


Figure 1.3: Vertical correlations of normalised differences between the observation and the NWP model background for bending angle. FY-3E top left, FY-3D top right and Metop-C bottom left.

2. Refractivity assessment

Figure 2.1 shows the normalised difference between the observed refractivity and the refractivity produced by the global NWP model forecast. The bias in the refractivity increases with height above 30 km which is not seen in the bending angle measurements. This behaviour is very similar to what we see in Metop-C with a slight deviation above 50 km, FY-3E having the larger bias. The bias is smaller for FY-3E when compared with FY-3D. There is a small reduction in the number of observations when going down from 30 km which is not as noticeable for the bending angle observations. Against FY-3D there is a reduction in the standard deviation between approximately 25-40 km which does not occur in the bending angle observations, Bowler (2019) also noted this between FY-3C and FY-3D. As for the bending angle observations, Metop-C has a smaller standard deviation.

FY-3E rising occultations have a smaller bias above 30 km than the setting occultations but the standard deviation is larger, which can be seen in figure 2.2.

Figure 2.3 shows the same $(O-B)/B$ but broken down by the different GNSS classifications available. For FY-3E; GPS and BeiDou are available. There is a small negative bias between 20 and 35 km for GPS observations. Observations from BeiDou begin to show a positive bias from around 35 km and this bias is slightly larger than that of GPS. BeiDou standard deviations are smaller than GPS below 35 km and are equal above.

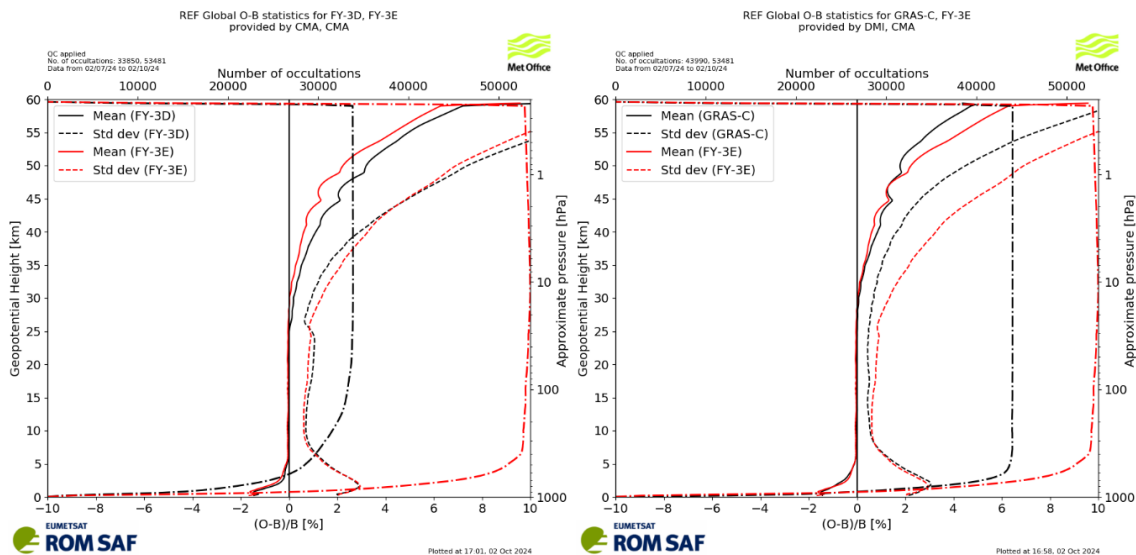


Figure 2.1: The bias and standard deviation of the normalised difference between the observation and the NWP model background forecast $(O-B)/B$ for refractivity. Left is FY-3D vs FY-3E and right is FY-3E vs Metop-C.

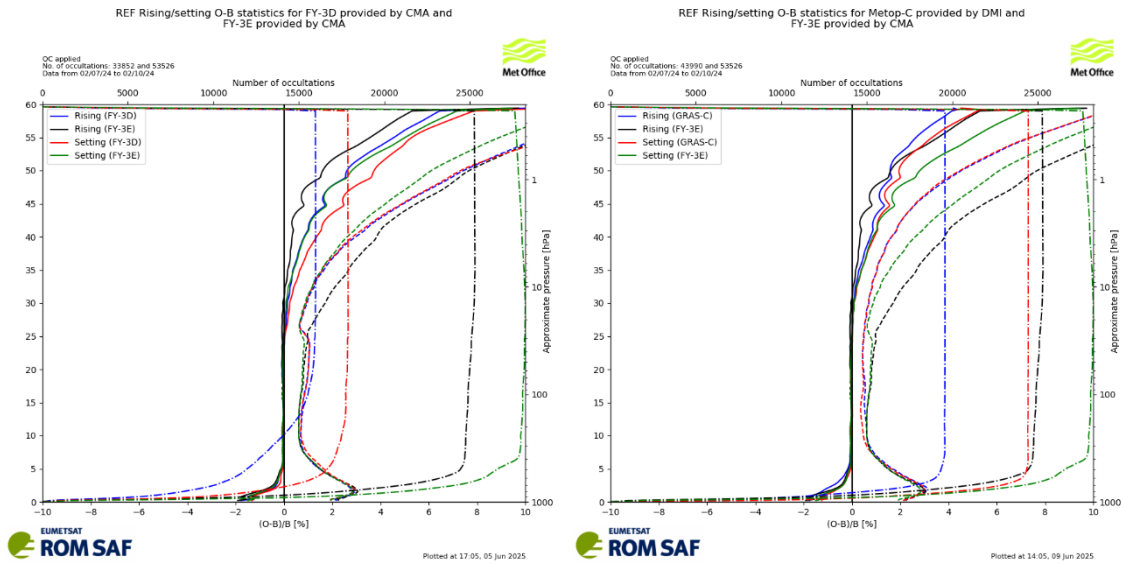


Figure 2.2: The bias and standard deviation of the normalised difference between the observation and the NWP model background forecast $(O-B)/B$ for refractivity for bending angle broken down into the rising and setting occultations. Left is FY-3D vs FY-3E and right is FY-3E vs Metop-C.

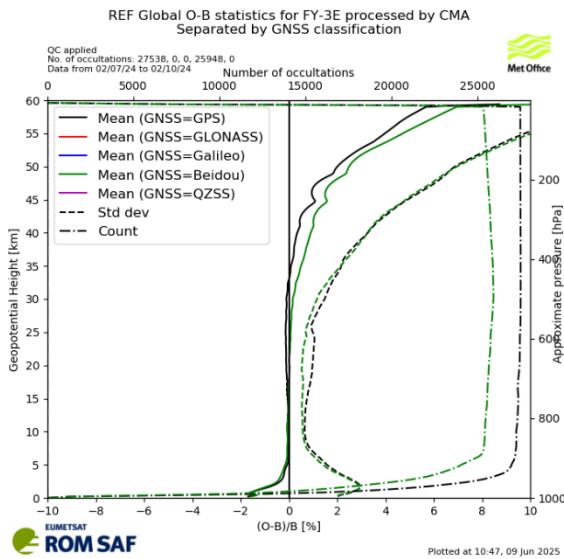


Figure 2.3: The bias and standard deviation of the normalised difference between the observation and the NWP model background forecast $(O-B)/B$ for refractivity for GPS and BeiDou observations.

The vertical correlations of the differences between the refractivity observed and that from the NWP model background is shown in Figure 2.4 for FY-3E, FY-3D and Metop-C. FY-3E and FY-3D show very similar vertical correlations, FY-3D having very slightly larger positive correlations. The FY satellites have longer vertical correlations particularly below 25 km.

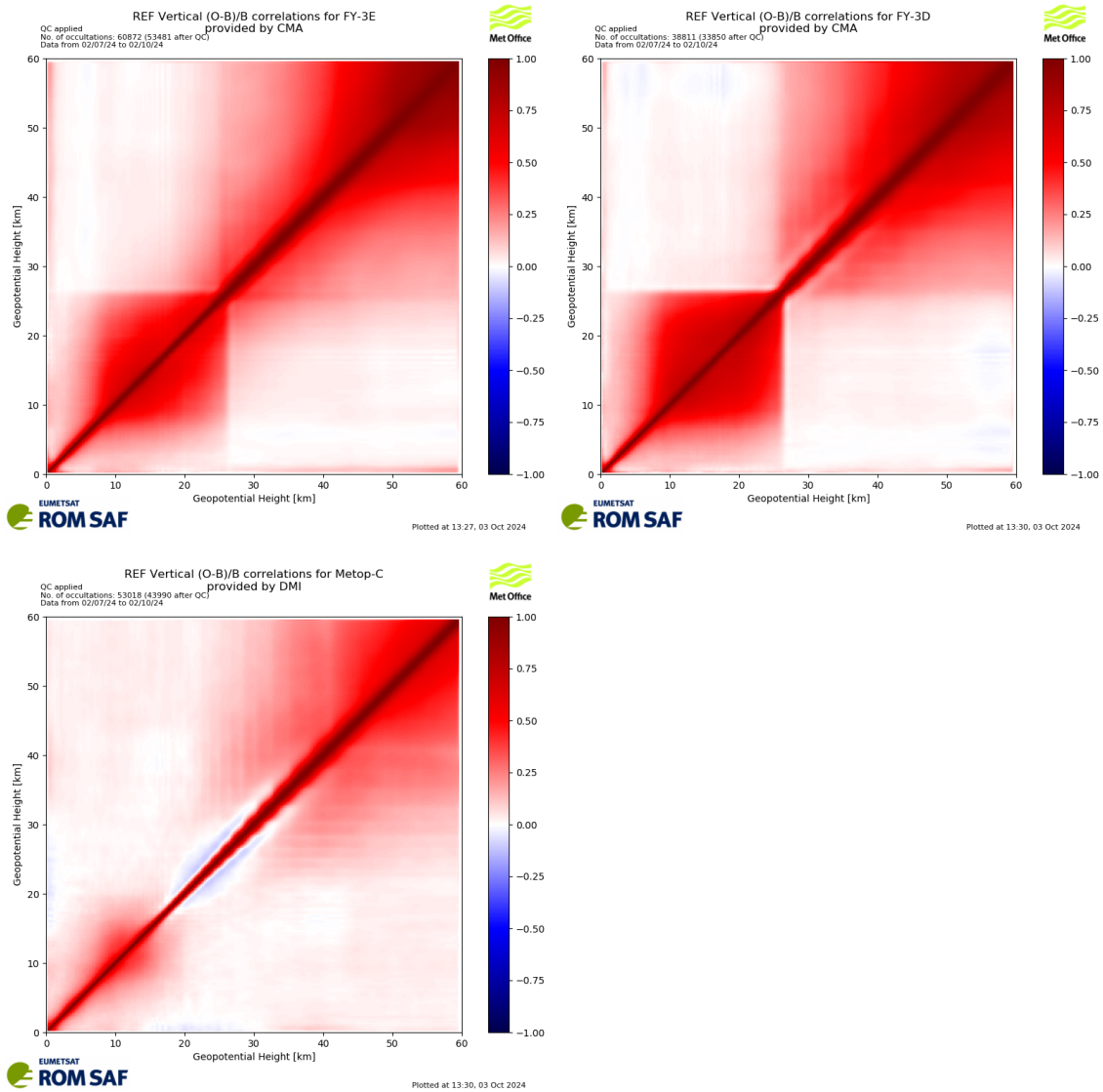


Figure 2.4: Vertical correlations of normalised differences between the observation and the NWP model background for refractivity. FY-3E top left, FY-3D top right and Metop-C bottom left.

3. Assimilation test

The impact of assimilating FY-3E observations into the Met Office’s operational Global NWP system was also tested. The test is setup using a replica of the operational system but run at a lower resolution to reduce compute requirements. The rising observations for FY-3E above 50 km were removed before assimilating as the bias indicated in Figure 1.2 was deemed to be too high. The results from this assimilation trial are compared against a control run which is the same apart from not including the extra FY-3E observations. The trial was run between the 1st April 2024 and 1st July 2024 using the Met Office’s global forecast model at N320 resolution (640x480 grid-points). The system runs a 7-day forecast every 12 hours and these are verified against ECMWF analyses and observations.

Figure 3.1 shows the scorecards of various NWP metrics at different forecast ranges. The green triangles indicate a decrease in the root mean square error (RMSE) and therefore an improvement in the forecast and blue triangles an increase in the RMSE. When the box is shaded it indicates that the result from that metric can be deemed to be statistically significant. As can be seen in Figure 3.1 the results from the assimilation trials of FY-3E do not show any noticeable features. The left plot shows verification against observations and in general has a negative slant with more blue triangles and squares. However, the size of these triangles and the lack of consistency of the affected lead times does not lead to a negative conclusion. The section that holds the most significance would be the NH_Z850 - NH_Z250 values as there is consistency between the heights affected and this is also across concurrent forecast lead times. However, the triangles here are very small indicating that it is only a small increase in the RMSE. Again, against the ECWMF analyses we see a similar result with a small number of negative impact blue triangles with the most noteworthy being the NH_Z500, NH_Z250 and NH_T_2m. There is also a small number of decreases in the RMS error particularly for temperatures in the tropics at 850 hPa and Southern Hemisphere temperatures at 500 and 250 hPa.

From the scorecards the overall picture would be a neutral impact as in general scorecards with overall percentage changes less than 0.1 % are not considered to be of significance.

The number of GNSS-RO observations being assimilated in the Met Office’s Global NWP model has increased in recent years. Although the impact from including FY-3E was neutral including it in the NWP system will improve resilience and the Met Office does expect to assimilate the data operationally.

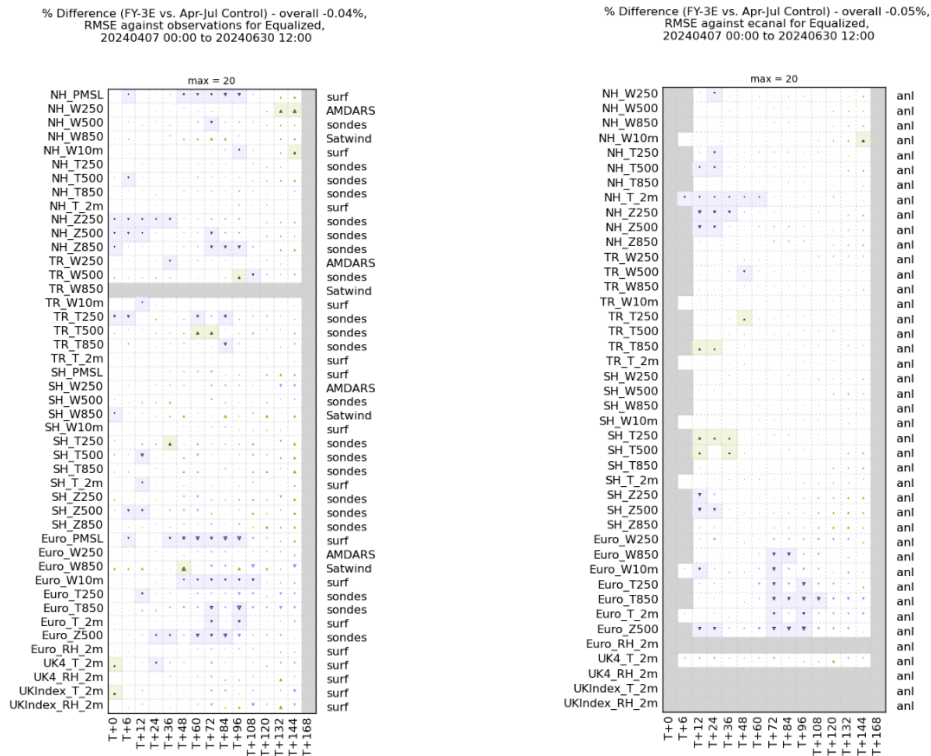


Figure 3.1: Verification results of assimilating FY-3E observations compared to a control test. Verification against observations (left) and verification against ECMWF (right). Green triangles indicate a reduction in the root-mean-square error of the forecast (improved), the size of the triangle demonstrating the size of the change. Blue indicates an increase in the RMS error of the forecast. A shaded box around the triangle indicates a statistically significant change.

4. Other notable features

The timeliness of the data received through the GTS is shown in Figure 4.1. The time taken for 90% of the observations to arrive for FY-3E is 5 hours and 15 minutes this is nearly two hours slower than FY-3D (3 hours and 6 minutes). This timeliness is substantially lower than Metop-C which provides 90% in 1 hour and 52 minutes. The green bars approximately indicate the observations which would be included in the “main” run of the Met Office’s global forecast model. To be included in the “main” run the observations need to arrive before 2 hours and 40 minutes after the nominal time of the assimilation window. There is also an update run which starts 6 hours after the nominal assimilation window so observations which arrive before this cut off will be included in the forecast. FY-3E during this month of analysis would have had around half the observations miss the 2 hour and 40 minute cutoff.

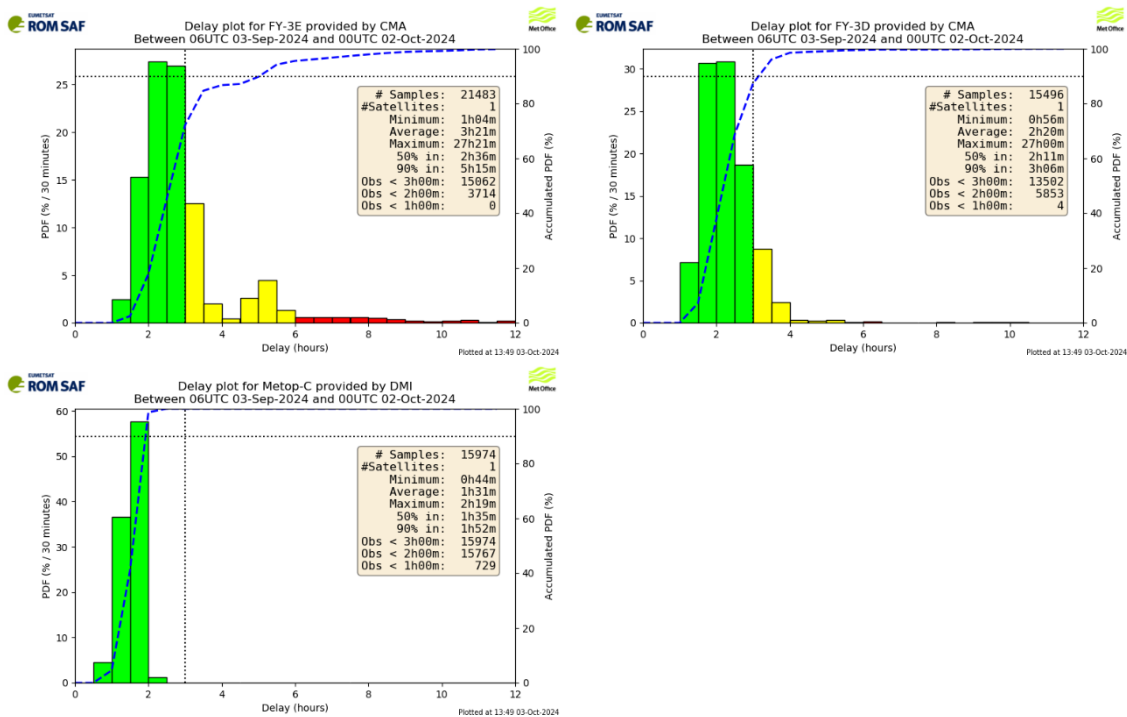


Figure 4.1: Time delay between the occultation observation being made and the receipt time in the Met Office’s observation database. FY-3E top left, FY-3D top right and Metop-C bottom left.

5. Conclusion

Overall, the quality of the observations from FY-3E agree with the quality of observations received from FY-3D. There are some differences in the FY-3E data, and these are:

- Rising bending angles above 50 km have a larger positive bias than either FY-3D or Metop-C.
- Bending angle standard deviations above 35 km are larger than Metop-C but smaller than FY-3D.
- Long-range bending angle vertical correlations between 10-26 km are slightly smaller for FY-3E compared to FY-3D.
- The bias in refractivity for FY-3E is smaller than FY-3D.
- The timeliness of FY-3E is slower than FY-3D by nearly 2 hours.

One trial has been run including FY-3E on top of the Met Offices current operational setup. Results from this trial were neutral to slightly negative. It is noted that during the preparations of this report there has been an upgrade to the processing introduced in January 2025. This has seen some improvements to the standard deviation between 10-25 km, with a small improvement to the bias around 20 km and small negative bias degradation around 10 km. However above 55 km the setting bending angle bias is above 8% and greater than 10% at 60 km.

6. References

Bowler N. (2019), Ref: SAF/ROM/METO/REP/RSR/035, Quality of FY-3D (available from: <https://rom-saf.eumetsat.int>)

ROM SAF (and GRAS SAF) Reports

SAF/GRAS/METO/REP/GSR/001	Mono-dimensional thinning for GPS Radio Occultation
SAF/GRAS/METO/REP/GSR/002	Geodesy calculations in ROPP
SAF/GRAS/METO/REP/GSR/003	ROPP minimiser – minROPP
SAF/GRAS/METO/REP/GSR/004	Error function calculation in ROPP
SAF/GRAS/METO/REP/GSR/005	Refractivity calculations in ROPP
SAF/GRAS/METO/REP/GSR/006	Levenberg-Marquardt minimisation in ROPP
SAF/GRAS/METO/REP/GSR/007	Abel integral calculations in ROPP
SAF/GRAS/METO/REP/GSR/008	ROPP thinner algorithm
SAF/GRAS/METO/REP/GSR/009	Refractivity coefficients used in the assimilation of GPS radio occultation measurements
SAF/GRAS/METO/REP/GSR/010	Latitudinal binning and area-weighted averaging of irregularly distributed radio occultation data
SAF/GRAS/METO/REP/GSR/011	ROPP 1D-Var validation
SAF/GRAS/METO/REP/GSR/012	Assimilation of Global Positioning System Radio Occultation data in the ECMWF ERA-Interim re-analysis
SAF/GRAS/METO/REP/GSR/013	ROPP PP validation
SAF/ROM/METO/REP/RSR/014	A review of the geodesy calculations in ROPP
SAF/ROM/METO/REP/RSR/015	Improvements to the ROPP refractivity and bending angle operators
SAF/ROM/METO/REP/RSR/016	Simplifying EGM96 undulation calculations in ROPP
SAF/ROM/METO/REP/RSR/017	Simulation of L1 and L2 bending angles with a model ionosphere
SAF/ROM/METO/REP/RSR/018	Single frequency radio occultation retrievals: impact on numerical weather prediction
SAF/ROM/METO/REP/RSR/019	Implementation of the ROPP two-dimensional bending angle observation operator in an NWP system
SAF/ROM/METO/REP/RSR/020	Interpolation artefact in ECMWF monthly standard deviation plots
SAF/ROM/METO/REP/RSR/021	5th ROM SAF User Workshop on Applications of GPS radio occultation measurements
SAF/ROM/METO/REP/RSR/022	The use of the GPS radio occultation reflection flag for NWP applications
SAF/ROM/METO/REP/RSR/023	Assessment of a potential reflection flag product
SAF/ROM/METO/REP/RSR/024	The calculation of planetary boundary layer heights in ROPP
SAF/ROM/METO/REP/RSR/025	Survey on user requirements for potential ionospheric products from EPS-SG radio occultation measurements
SAF/ROM/METO/REP/RSR/026	Estimates of GNSS radio occultation bending angle and refractivity error statistics
SAF/ROM/METO/REP/RSR/027	Recent forecast impact experiments with GPS radio occultation measurements
SAF/ROM/METO/REP/RSR/028	Description of wave optics modelling in ROPP-9 and suggested improvements for ROPP-9.1
SAF/ROM/METO/REP/RSR/029	Testing reprocessed GPS radio occultation datasets in a re-analysis system
SAF/ROM/METO/REP/RSR/030	A first look at the feasibility of assimilating single and dual frequency bending angles

SAF/ROM/METO/REP/RSR/031	An initial assessment of the quality of RO data from KOMPSAT-5
SAF/ROM/METO/REP/RSR/032	An initial assessment of the quality of RO data from Metop-C
SAF/ROM/METO/REP/RSR/033	Some science changes in ROPP-9.1
SAF/ROM/METO/REP/RSR/034	An initial assessment of the quality of RO data from Metop-C
SAF/ROM/METO/REP/RSR/035	An initial assessment of the quality of RO data from FY-3D
SAF/ROM/METO/REP/RSR/036	An initial assessment of the quality of RO data from PAZ
SAF/ROM/METO/REP/RSR/037	6th ROM SAF User Workshop
SAF/ROM/METO/REP/RSR/038	An initial assessment of the quality of RO data from COSMIC-2
SAF/ROM/METO/REP/RSR/039	Impacts of RO mission differences on trends in multi-mission data records
SAF/ROM/METO/REP/RSR/040	Anomalous GRAS radio occultations
SAF/ROM/METO/REP/RSR/041	Assessment of sensitivity of the ROM SAF 1D-Var solutions to various error covariance choices
SAF/ROM/METO/REP/RSR/042	A one-dimensional variational ionospheric retrieval for truncated GNSS Radio Occultation measurements
SAF/ROM/METO/REP/RSR/043	Applying the ROPP ionospheric 1D-Var retrieval to Metop extension data
SAF/ROM/METO/REP/RSR/044	TBA
SAF/ROM/METO/REP/RSR/045	TBA
SAF/ROM/METO/REP/RSR/046	8th EUMETSAT ROM SAF user workshop on GNSS radio occultation measurements
SAF/ROM/METO/REP/RSR/047	An initial assessment of the quality of RO data from FY-3E

ROM SAF Reports are accessible via the ROM SAF website: <https://rom-saf.eumetsat.int/>